International Journal of Optics and Applications 2019, 8(2): 21-31
DOI: 10.5923/j.optics.20190802.01

Wideband Electromagnetic Wave Generation via Supercontinuum Formation in Infrared-Resonant Optical Microcavities

Özüm Emre Aşırım*, Mustafa Kuzuoğlu

Department of Electrical and Electronics Engineering, Middle East Technical University, Ankara, Turkey

Abstract High intensity wave generation is hard to achieve in certain frequency intervals such as the terahertz frequency range and the ultraviolet frequency range. In this paper we present a numerical study for ultra-wideband spectral broadening (supercontinuum formation) and wideband electromagnetic wave generation in a small infrared-resonant optical microcavity. It was observed that at a given intracavity intensity, spectral broadening occurs profoundly near the resonance frequency of the cavity material, and the broadening effect drastically weakens when the excitation frequency is away from the resonance frequency. A numerical example is presented for an intense, near resonance, infra-red frequency excitation, and the resulting spectral broadening is investigated in the terahertz-ultraviolet frequency range. This numerical example is repeated for some other resonance frequency values that are gradually further from the infrared frequency range, and the resulting cessation of the spectral broadening process is illustrated. It is found that, for an infrared-resonant optical microcavity, supercontinuum can be generated under intense near-resonance excitation and spectrally ultra-tunable electromagnetic waves can be generated at the cavity output with the use of a switch controlled bandpass filter.

Keywords Spectral broadening, Resonance frequency, Supercontinuum, Harmonic generation, Nonlinear media

1. Introduction

When a nonlinear medium is excited by a wave of very high intensity, spectral broadening may occur depending on the length of the medium and the strength of nonlinearity of the medium [1-5]. The nonlinear medium that is used for spectral broadening is often chosen as a long optical fiber. Although, when the excitation intensity is of very high intensity, one can use a piece of bulk nonlinear crystal such as glass to observe spectral broadening. The required intensity to observe a significant spectral broadening by using a piece of bulk nonlinear crystal of a few centimeters of length, is on the order of GW/cm^2. Such high intensities are achievable by using *Q switched lasers* or *Mode locked lasers*, and usually have pulse widths ranging from femtoseconds to picoseconds. The degree of spectral broadening depends mainly on the second order nonlinear electric susceptibility ($\chi^{(2)}$) and/or the third order nonlinear electric susceptibility ($\chi^{(3)}$) of the nonlinear crystal [6].

Achieving a significantly broadened spectrum in the THz frequency range or in the UV (Ultraviolet) frequency range is quite difficult as it is difficult to generate high power electromagnetic radiation in these parts of the spectrum. Modern lasers can generate very high-power laser beams in the infra-red region of the spectrum, but not as much in the THz or UV region of the spectrum. Therefore, it is of interest to search for a technique to generate high power radiation in the THz/UV range along with a continuously broadened spectrum.

In the last decade, the vast majority of supercontinuum generation research has focused on optical fibers and their modification for achieving a wider supercontinuum, mainly photonic crystal fibers. Existing literature on supercontinuum generation is about the engineering of the constitutive parameters, structure, and geometry of optical/photonic crystal fibers to achieve a more extensive supercontinuum generation, such as those mentioned in [7-17]. Some research has focused on the pulse parameters of the excitation laser beams such as those as mentioned in [13,14]. Although not always mentioned or detailed in the existing literature, we have deduced that all these engineering attempts tend to modify either the resonance frequency of the engineered fiber structure, or the spectrum of the excitation (laser pulse). The relation between the excitation frequency and the resonance frequency has not been thoroughly investigated. In this paper we want to show that by carefully selecting the excitation frequency to be close to the resonance frequency (f_0) of the medium of propagation, we can greatly increase the extent of spectral

* Corresponding author:
ozumasirim88@gmail.com (Özüm Emre Aşırım)
Published online at http://journal.sapub.org/optics

broadening and may use this technique to generate high intensity waves in a wide frequency band that ranges from the terahertz region to the ultraviolet frequency region.

If we assume that the nonlinear susceptibility terms ($\chi^{(2)}$, $\chi^{(3)}$) are isotropic and frequency independent, then the electric field (E) of the high intensity wave that undergoes spectral broadening in a non-centrosymmetric nonlinear dielectric media is given as [1]

$$\nabla^2(E) - \mu_0\varepsilon_0\left(1+\chi^{(1)}\right)\frac{\partial^2(E)}{\partial t^2} = \mu_0\varepsilon_0\left(\frac{\partial^2\{\chi^{(2)}(E)^2+\chi^{(3)}(E)^3\}}{\partial t^2}\right) \quad (1)$$

μ_0: Free space permeability, ε_0: Free space permittivity, E: Electric field, $\chi^{(K)}$: Kth order susceptibility

This formulation states that the second and the third harmonics of the excitation frequency will be generated after a certain propagation time as evident by the right side of the equation. If the excitation intensity is sufficiently high, even nonnegligible fourth and sixth harmonics may be generated. But since ultra-high intensity waves (laser pulses) have very short durations [18,19] (on the order of picoseconds or femtoseconds), the nonlinear dielectric response must be modeled as a dispersive one. The inclusion of dispersion in the analysis is what enables us to observe a continuously broadened spectrum [20,21]. Therefore, in order to investigate the spectral broadening of a laser pulse in a nonlinear media, we need to be careful and accurate on how to include dispersion in the nonlinear wave equation. Our aim is to use a mathematical description of the wave equation that accounts for the resonance frequency. In order to use a simple and a clear mathematical model, we will model a separate differential equation for the electric charge polarization density and solve it in parallel with the wave equation, as described in the following section.

2. Wave Propagation in Nonlinear Dispersive Media

When the wave that propagates through a dispersive medium has a very high power, nonlinearity arises. In this case, we must use a model that handles dispersion and nonlinearity simultaneously [22,23]. In order to model the nonlinear dispersive media, we solve the wave equation in parallel with the nonlinear equation of motion of an electron cloud as given below in Eq.2a and Eq.2b [24,25]:

$$\nabla^2 E - \mu_0\varepsilon_\infty\frac{\partial^2 E}{\partial t^2} = \mu_0\sigma\frac{\partial E}{\partial t} + \mu_0\frac{\partial^2 P}{\partial t^2}. \quad (2a)$$

$$\frac{\partial^2 P}{\partial t^2} + \gamma\frac{\partial P}{\partial t} + {\omega_0}^2 P - \frac{{\omega_0}^2}{Ned}P^2 - \frac{{\omega_0}^2}{N^2e^2d^2}P^3 = \frac{Ne^2}{m}E. \quad (2b)$$

P: Charge polarization density (Coulomb/m^2), e: Electron charge, m: Electron mass, N: Electron density

ε_∞: Background (infinite frequency band) permittivity, γ: Natural damping coefficient of a medium, d: Atomic diameter,

μ_0: Free space permittivity, ω_0: Angular resonance frequency of a medium, σ: Electric conductivity (Siemens/m)

In Eq. (2b) we have made an expansion up to the third order of the nonlinear charge polarization density as higher order terms will be negligibly small [26,27]. Note that equations (2a) and (2b) are coupled to each other and need to be solved simultaneously. We will analyze the effect of the resonance frequency (f_0) of the cavity medium on spectral broadening and harmonic generation in an optical cavity which has an optical isolator as the left cavity wall and a switch controlled bandpass filter as the right cavity wall as shown in figure 1.

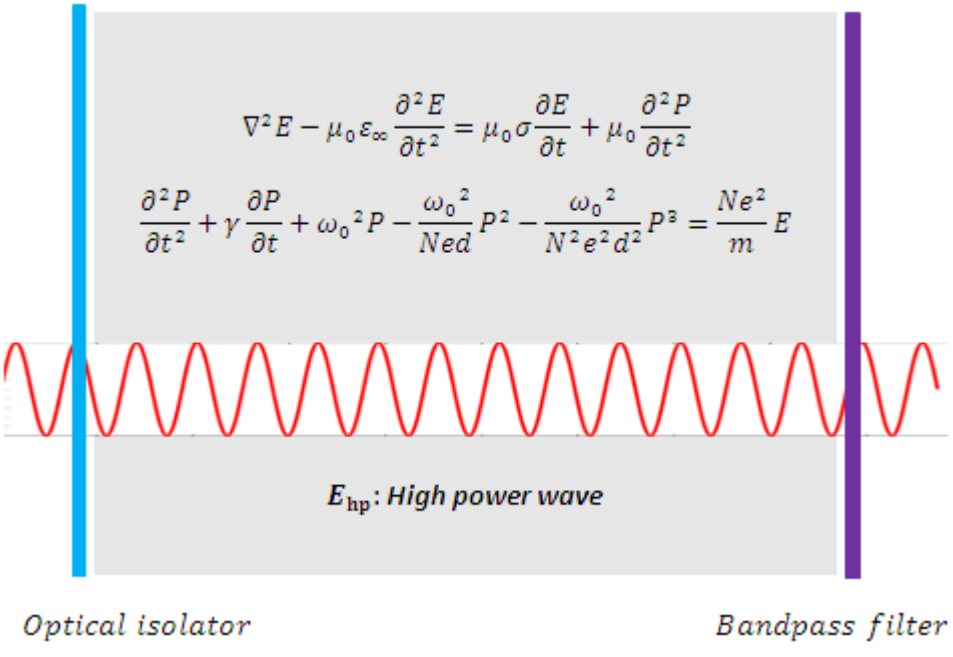

Figure 1. Modeling of wave propagation in a nonlinear dispersive medium inside a cavity

We discretize and solve the equations (2a,2b) using the finite difference time domain method. Equations (2a,2b) are discretized as follows:

$$\frac{E(i+1,j)-2E(i,j)+E(i-1,j)}{\Delta x^2}-\mu_0\varepsilon_\infty(i,j)\frac{E(i,j+1)-2E(i,j)+E(i,j-1)}{\Delta t^2}=\mu_0\sigma(i,j)\frac{E(i,j)-E(i,j-1)}{\Delta t}+\mu_0\frac{P(i,j+1)-2P(i,j)+P(i,j-1)}{\Delta t^2}. \quad (3a)$$

$$\frac{P(i,j+1)-2P(i,j)+P(i,j-1)}{\Delta t^2}+\gamma\frac{P(i,j)-P(i,j-1)}{\Delta t}+{\omega_0}^2\big(P(i,j)\big)-\frac{{\omega_0}^2}{Ned}\big(P(i,j)\big)^2-\frac{{\omega_0}^2}{N^2e^2d^2}\big(P(i,j)\big)^3=\frac{Ne^2}{m}\big(E(i,j)\big). \quad (3b)$$

x: spatial coordinate, t: time, i: spatial coordinate index, j: time index

$$x=i\Delta x, t=j\Delta t,\ x(i+1,j)-x(i,j)=\Delta x\,,$$
$$t(i,j+1)-t(i,j)=\Delta t$$

By solving equations (2a,2b) simultaneously, along with the initial condition and the boundary conditions of a given problem, we can get the time variation of E at any point in one dimensional space.

3. Simulation Results

Simulation 1: The high-power wave $\boldsymbol{E}$ is propagating inside a cavity that has two reflecting walls on the left and right side. The reflecting wall on the left side can be thought as an optical isolator, the one on the right side represents a switch controlled band-pass filter with a frequency dependent reflection coefficient.

$$\boldsymbol{E}(x=0.1\mu m,t)=6\times10^7\sin(2\pi(2.2\times10^{14})t)\ V/m\,,\quad for\ \ 0\le t\le 30ps$$

Resonance frequency of the medium: f_0*; Damping rate of the medium:* $\gamma=1\times10^{10}\ Hz$

Dielectric constant of the medium $(\varepsilon_\infty)=12$ $(\mu_\infty=1)$

Spatial range of the simulation domain: $0\le x\le 15\mu m$*; Dielectric medium range:* $0.2\mu m<x<9.8\mu m$

Left cavity wall location: $x=0\mu m$*, Right cavity wall location:* $x=10\mu m$

Electron density of the nonlinear medium: $N=3.5\times10^{28}/m^3$*, Atomic diameter:* $d=0.3\ nm$

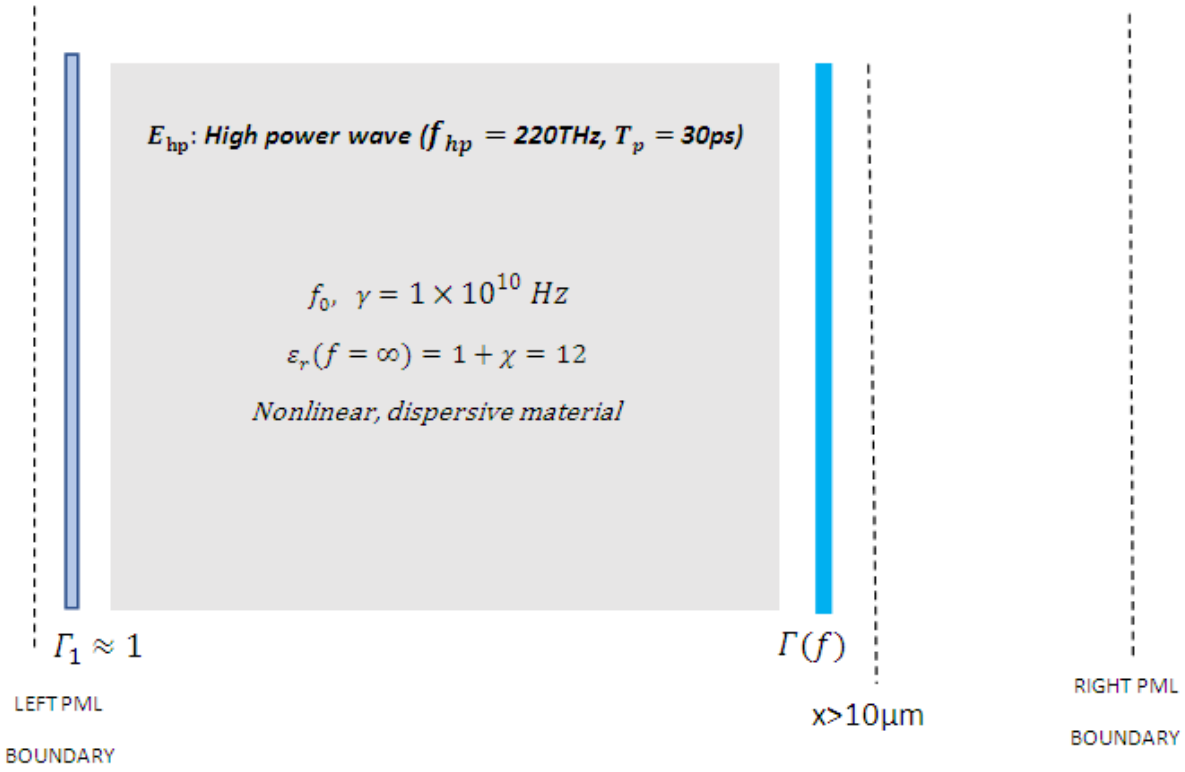

Figure 2. Configuration of the cavity

The propagation of the high-power wave inside the cavity is governed by equations (3a,3b).

Initial conditions: $P(x,0)=P'(x,0)=E(x,0)=E'(x,0)=0$ (the prime sign indicates the time derivative)

Boundary conditions:

$E(x=10\mu m,t)=E(x=0\mu m,t)=0\ for\ \ 0<t<30ps$

For an input high power wave of frequency f_{hp}=220THz (one of the Nd:YAG laser emission frequencies), we solve equations (3a,3b) for each resonance frequency value from 10THz to 1500THz, and compute the maximum wave amplitude that is reached inside the cavity for 0<t<30ps, as shown below in figure 3.

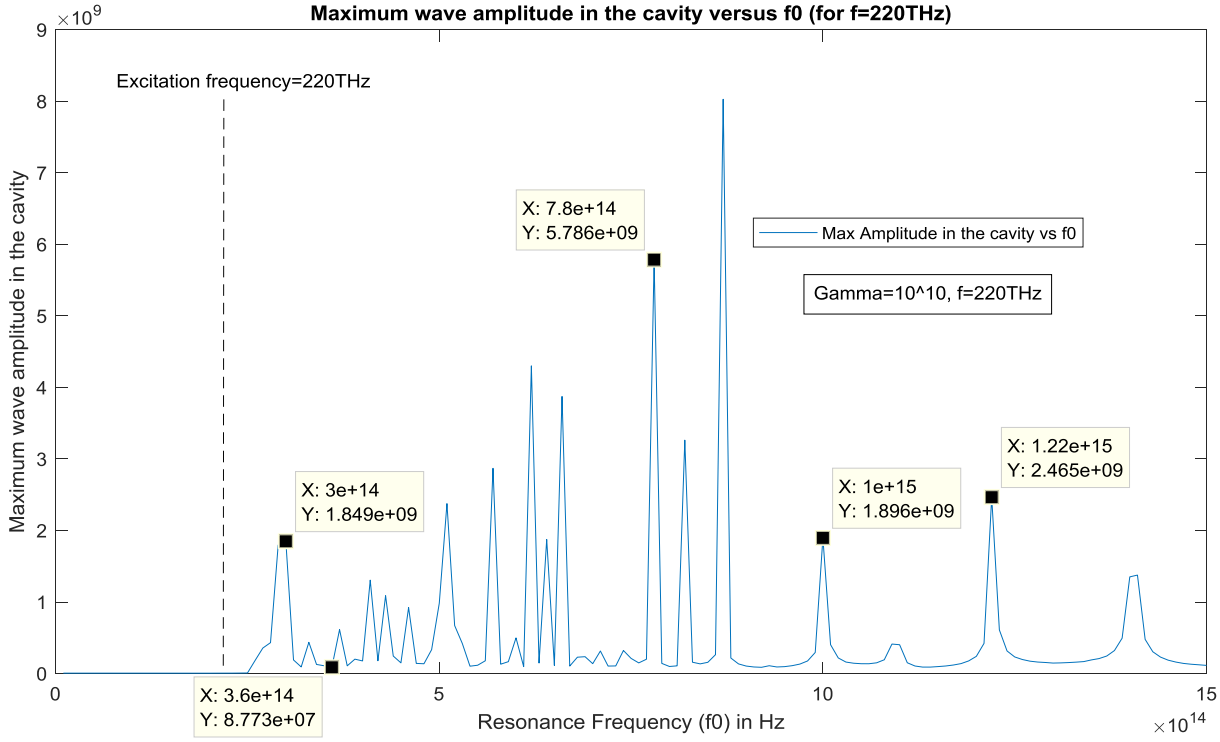

Figure 3. Maximum wave amplitude in the cavity versus the resonance frequency (f_0), for f_{hp}=220THz and $\gamma = 1 \times 10^{10} Hz$. Our spectral broadening measurements are made at the indicated resonance frequencies

Note that, parameters such as the background permittivity ε_∞ and the conductivity σ are assumed to be time independent, as the dispersion of the media is governed by the nonlinear electron cloud motion equation (eq.2b) rather than being incorporated into the medium parameters in a standalone wave equation. The damping coefficient γ is the inverse of the charge polarization lifetime of the electrons, which is a material specific constant rather than a time dependent quantity.

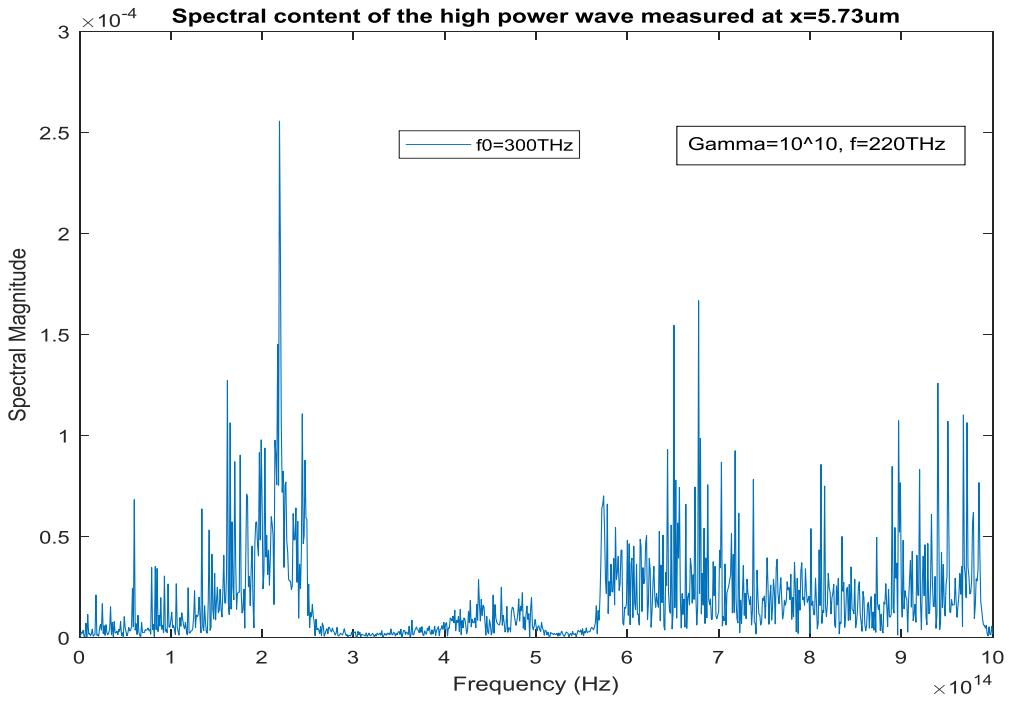

Figure 4. Spectrum of the high-power wave as computed inside the cavity at x=5.73μm for $f_0 = 300THz$

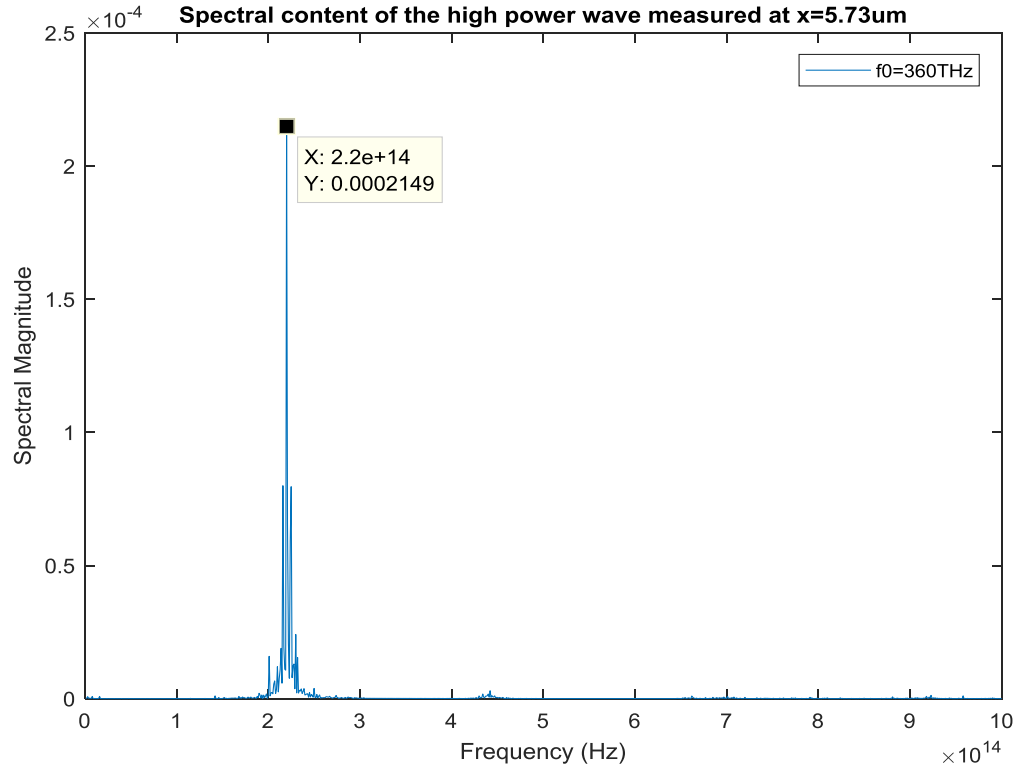

Figure 5. Spectrum of the high-power wave as computed inside the cavity at x=5.73μm for $f_0 = 360THz$

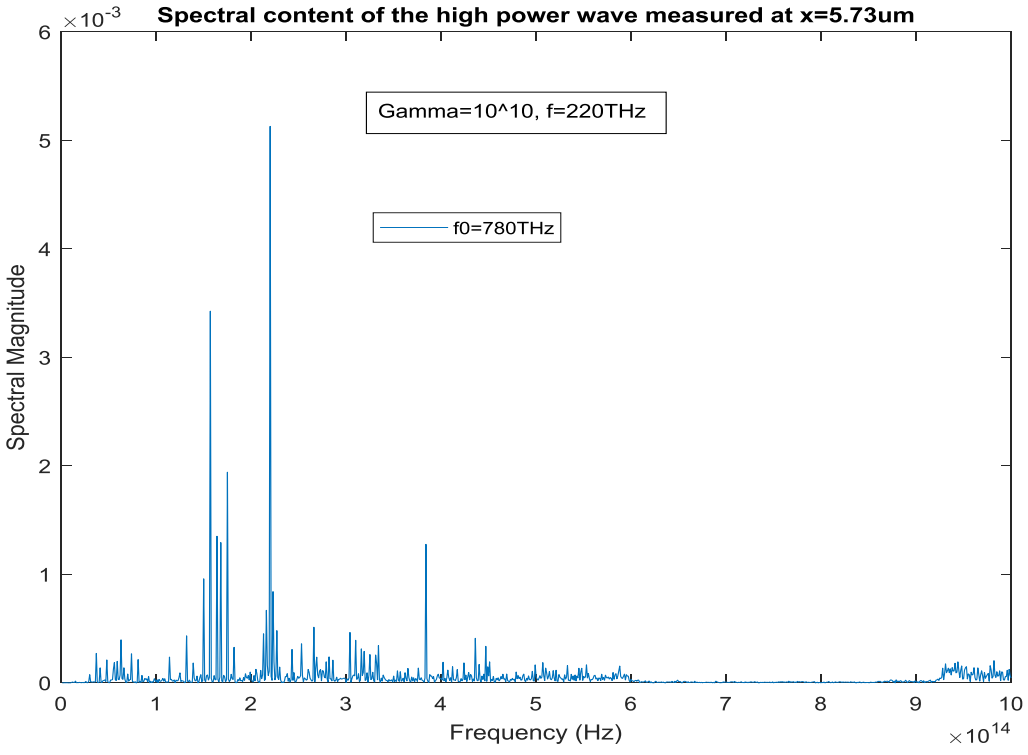

Figure 6. Spectrum of the high-power wave as computed inside the cavity at x=5.73μm for $f_0 = 780THz$

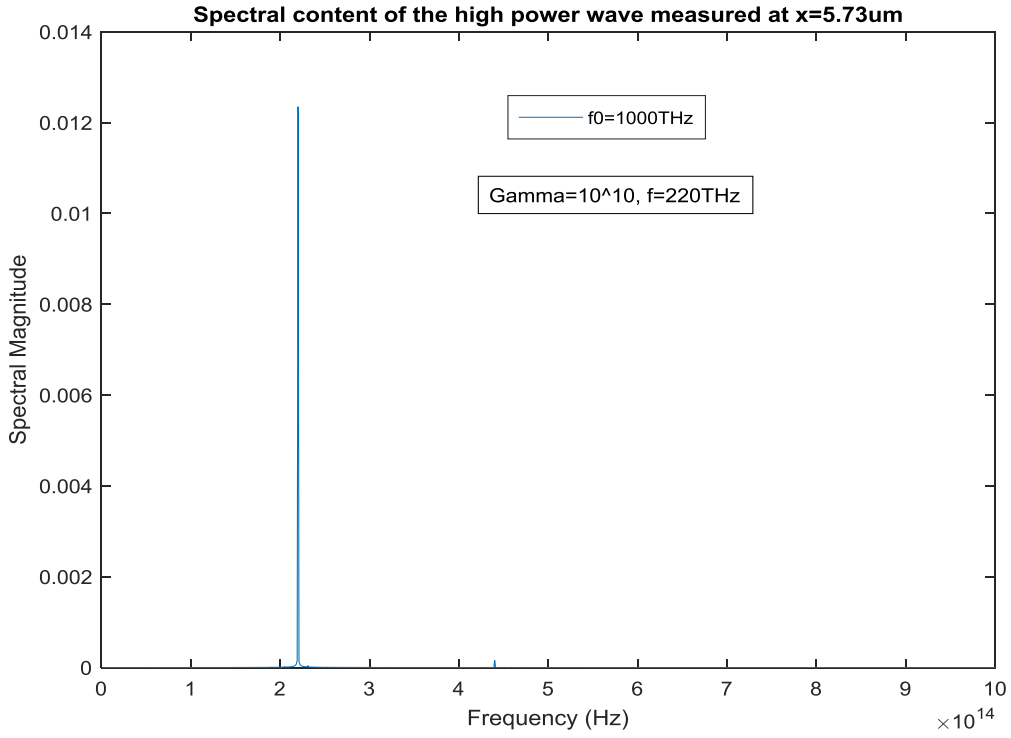

Figure 7. Spectrum of the high-power wave as computed inside the cavity at x=5.73μm for $f_0 = 1000THz$

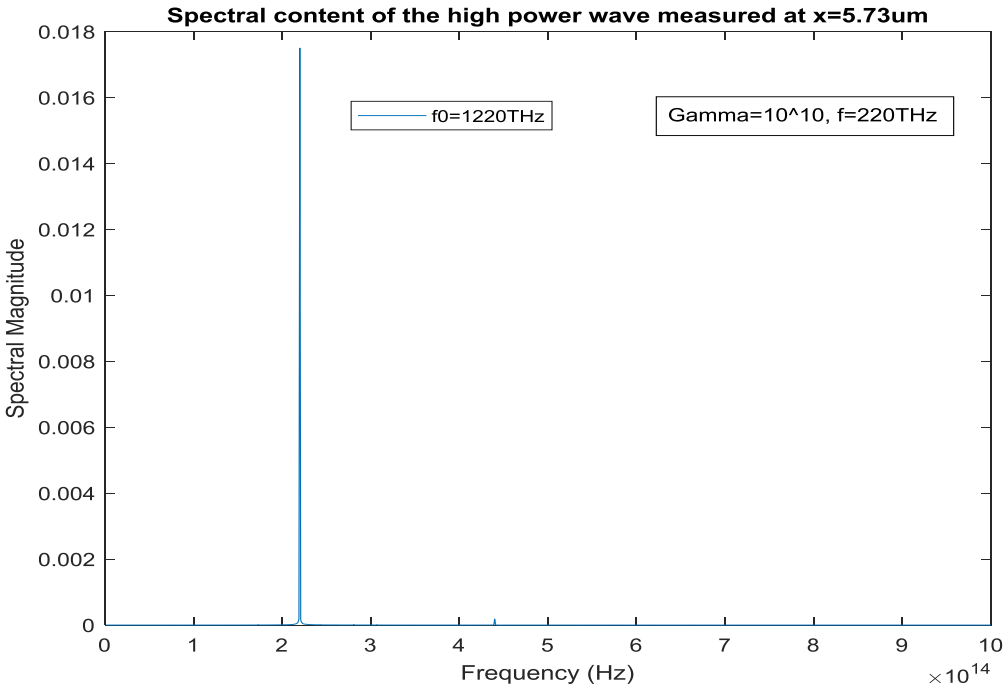

Figure 8. Spectrum of the high-power wave as computed inside the cavity at x=5.73μm for $f_0 = 1220THz$

There are many peak values of the maximum wave amplitude that can be achieved as shown in figure 3. As an initial choice, we choose the nearest amplitude peak of $f_0 = 300THz$ and investigate the spectrum of the wave in the cavity. As we can see from figure 4, the spectrum of the wave encompasses the whole band from 10THz to 1000THz (from THz to UV), this is called a supercontinuum as the spectral broadening is ultrawide. The generation of the

supercontinuum is due to the intracavity wave amplitude being high and most importantly due to the resonance frequency being close to the excitation frequency.

If we look at the spectral broadening at $f_0 = 360THz$ (figure 5), we can see that the broadening at $f_0 = 360THz$ is much less significant than the broadening at $f_0 = 300THz$ even though we are still close to the excitation frequency. This is because the intracavity wave amplitude is much smaller at $f_0 = 360THz$.

For the amplitude peak at $f_0 = 780THz$, the spectral broadening is significant (figure 6), but not as profound as in the case of $f_0 = 300THz$, even though the peak at $f_0 = 780THz$ has a much higher spectral amplitude. This is due to the increased spectral distance from the excitation frequency.

For $f_0 = 1000THz$ there is no spectral broadening at all (fig 7), even though the amplitude of the peak at $f_0 = 1000THz$ is almost the same with the peak at $f_0 = 300THz$. Similarly, for the amplitude peak at $f_0 = 1220THz$ there is no spectral broadening (fig 8), even though the amplitude of the peak at $f_0 = 1220THz$ is higher than the amplitude of the peak at $f_0 = 300THz$. This is because we are now too far from the excitation frequency to observe any broadening.

Therefore, we conclude that, as the intracavity peak amplitude gets higher, and as the excitation frequency gets closer to the resonance frequency of the medium, the extent of the spectral broadening increases, in other words, the peak power in the cavity becomes more distributed along the spectrum.

Now let us go back to the analysis at $f_0 = 300THz$ where the spectral broadening is the most prominent. Once the spectral broadening occurs everywhere in a desired frequency range, as in the case of figure 4, we can use a bandpass filter in order to obtain a high-power output wave at a certain frequency. For example, we can obtain a high-power output in the ultraviolet frequency range or in the far-infrared frequency range. In order to obtain an output at a desired frequency, we need to adjust the frequency response of the bandpass filter accordingly. Consider the following configuration, assume that we have the fixed values of $f_{hp} = 2.2 \times 10^{14} Hz$, $f_0 = 3 \times 10^{14} Hz$, and $\gamma = 1 \times 10^{10} Hz$. The right cavity wall is a switch controlled bandpass filter and for a wave frequency (f), the magnitude frequency response of the filter is chosen as

$$\Gamma(f') = \begin{cases} 1 \; for \; all \; f' \; , for \; 0 \le t \le 30ps \\ 1 - e^{-(\frac{(f'-f)}{\sqrt{2}THz})^2} \; , for \; t > 30ps \end{cases}$$

The left cavity wall is an ideal optical isolator, which acts as a perfect transmitter from the left side and as a perfect reflector from the right side. Optical isolators are generally used for avoiding high power reflections to prevent optical damage. Since we are only interested in what is going on inside the cavity (the right side of the isolator), we model the optical isolator as a perfect reflector.

After the spectral broadening has occurred (t>30ps), the resulting cavity/filter output for each frequency is plotted in figure 9 below, for the configuration described above.

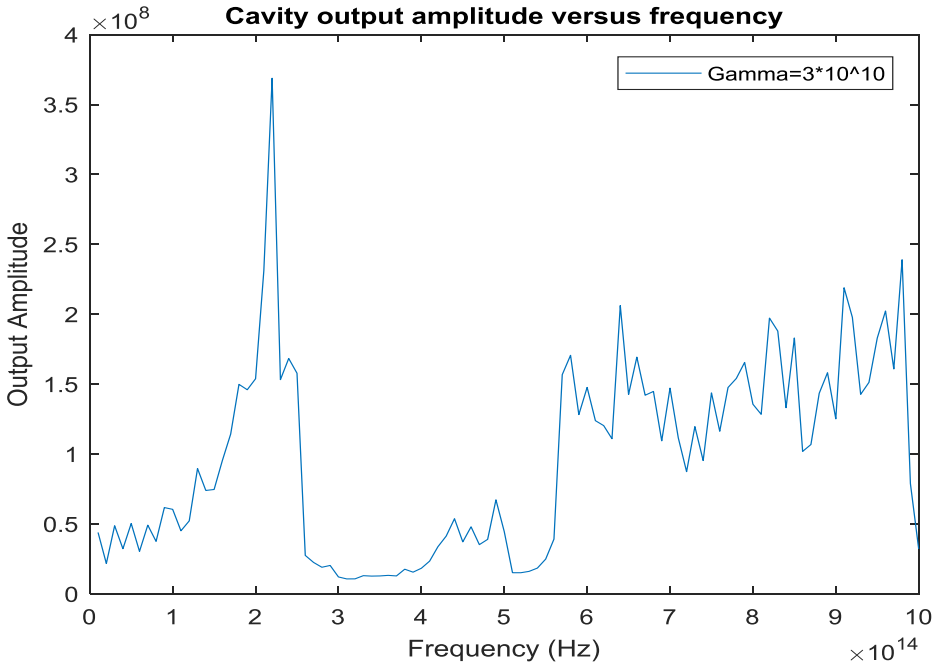

Figure 9. Cavity output amplitude versus desired output frequency

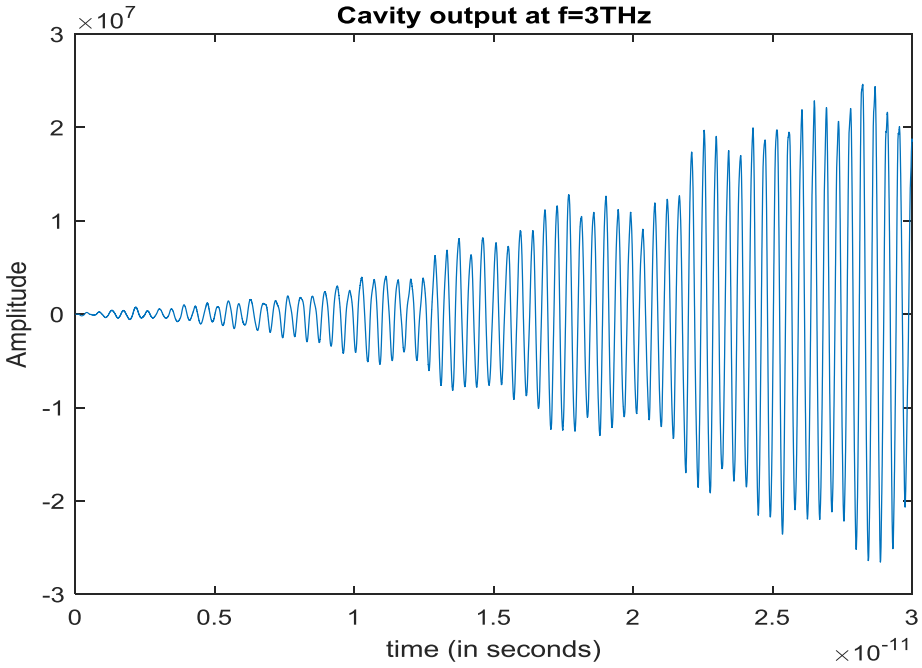

Figure 10. Amplitude variation of the cavity output at 3THz versus time

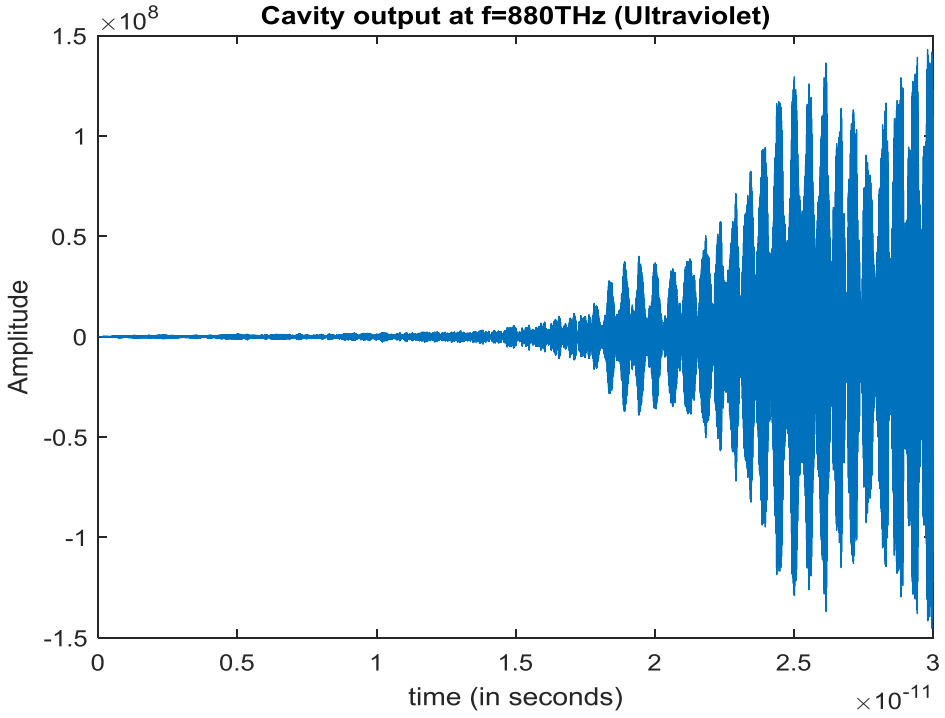

Figure 11. Amplitude variation of the cavity output at 880THz versus time

4. Conclusions

Wideband spectral broadening or supercontinuum formation can occur inside a small infrared-resonant microcavity, under high intracavity wave intensity, provided that the resonance frequency of the cavity medium is close to the excitation frequency. As the intensity of the wave increases and as the resonance frequency gets closer to the excitation frequency, the spectral broadening occurs at a greater extent. Once the spectral broadening occurs at a target bandwidth, we can obtain a high-power output at a desired frequency, using a switch controlled optical bandpass filter. This allows us to generate intense electromagnetic waves in the frequency ranges where obtaining a high-intensity output is difficult, such as the terahertz range (1THz-10THz) or the ultraviolet frequency range.

5. Appendix: Validation of the Computational Model

Simulation 2: (Second harmonic generation (SHG))

This simulation aims to compare our computational model with the theoretical results given in [1,4].

The input field $\boldsymbol{E}$ is generated at x=2.5μm. It has an amplitude of A_1V/m and a frequency of 300THz.

$$\boldsymbol{E}(x = 2.5\mu m, t) = A_1 \times \sin(2\pi(3 \times 10^{14})t)\ V/m$$

Simulation parameters: $0 \le x \le 10\mu m, 0 \le t \le 60ps$

Resonance frequency of the nonlinear medium: $f_0 = 1.1 \times 10^{15} Hz$

Damping rate of the nonlinear medium: $\gamma = 1 \times 10^{12} Hz$

Dielectric constant of the nonlinear medium $(\varepsilon_\infty) = 10$

Nonlinear dielectric medium spatial range: $3.33\mu m < x < 6.66\mu m$

The values of f_0 and γ given above are typical values for solid media. Computationally, the second harmonic generation efficiency results are obtained by solving equations (3a,3b).

For $0 \le t \le t_{max}$, the computational formula for second harmonic generation efficiency is

$$\eta_{computational} = \frac{\text{Intensity of the } second\ harmonic\ (2\omega) \text{ of the wave at t} = t_{max}}{\text{Intensity of the } first \text{ harmonic } (\omega) \text{ of the wave at t} = 0}$$

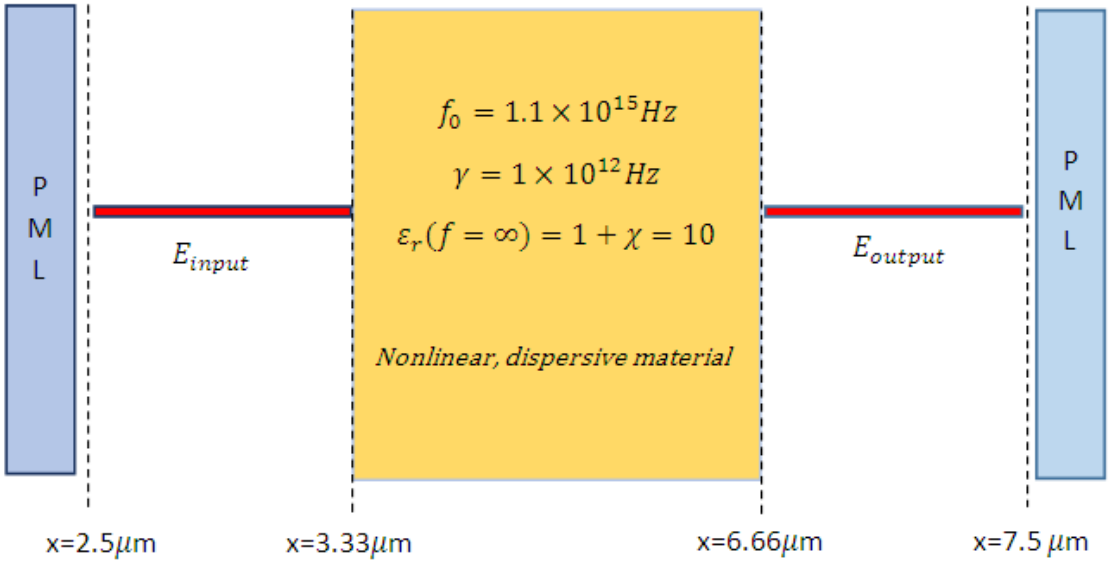

Figure 12. A high amplitude infra-red laser beam passing through a nonlinear dispersive medium

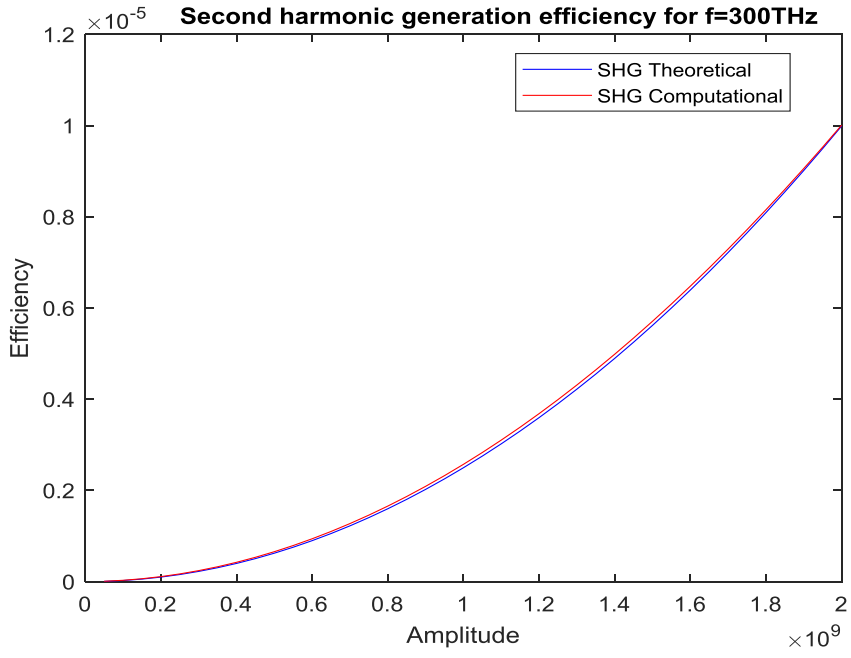

Figure 13. Comparison of the second harmonic generation (SHG) efficiencies for f=300THz

The experimentally verified theoretical second harmonic generation efficiency formula is given as

$$\eta = (\tanh\sqrt{d^2 n^4 \omega^2 c\varepsilon_0 {A_1}^2 L^2})^2 \quad (4)$$

d = Nonlinear coefficient; n = refractive index; L = length of the nonlinear media; c = Speed of light

ω = Input frequency (first harmonic); A_1= Input wave electric field amplitude

Assume that we have the following values of the parameters

$A_1 = 1 \times 10^9 V/m$, f=300THz, L=3.3333µm, n=3.1623 ($\varepsilon_r = 10$)

For these values, the theoretical result at $A_1 = 1 \times 10^9 V/m$ becomes almost equal to our computational result for a nonlinearity coefficient of $d = 4.93 \times 10^{-22}$. Therefore, we estimate this value as our nonlinearity coefficient and see if the results still agree for all other input amplitudes. The resulting comparison is shown in figure 13.

REFERENCES

[1] Boyd Robert. W., Nonlinear Optics, Academic Press, New York, 2008.

[2] Fox Mark, Optical properties of solids, Oxford University Press, New York, 2002.

[3] Balanis Constantine. A., Advanced Engineering Electromagnetics, John Wiley & Sons, New York, 1989.

[4] Bahaa E. A. Saleh, Malvin Carl Teich, Fundamentals of Photonics,Wiley-Interscience, New York, 2007.

[5] Silfvast William.T., Laser Fundamentals, Cambridge University Press, New York, 2004.

[6] Taflove Allen, Hagness Susan.C., Computational Electrodynamics: The Finite-Difference Time-Domain Method, Artech House, Boston, 2005.

[7] J. M. Dudley and J. R. Taylor, "Ten years of nonlinear optics in photonic crystal fibre", Nature Photon. 3, 85 (2009), doi:10.1038/nphoton.2008.285.

[8] X. Hu et al., "High average power, strictly all-fiber supercontinuum source with good beam quality", Opt. Lett. 36 (14), 2659 (2011), doi:10.1364/OL.36.002659.

[9] A. M. Heidt et al., "Limits of coherent supercontinuum generation in normal dispersion fibers", J. Opt. Soc. Am. B 34 (4), 764 (2017), doi:10.1364/JOSAB.34.000764.

[10] R. A. Martinez et al., "Mid-infrared supercontinuum generation from 1.6 to >11 µm using concatenated step-index fluoride and chalcogenide fibers", Opt. Lett. 43 (2), 296 (2018), doi:10.1364/OL.43.000296.

[11] V. T. Hoang et al., "All-normal dispersion supercontinuum generation in photonic crystal fibers with large hollow cores infiltrated with toluene", Optical Materials Express 8 (11), 3568 (2018), doi:10.1364/OME.8.003568.

[12] V. T. Hoang et al., "Supercontinuum generation in an all-normal dispersion large core photonic crystal fiber infiltrated with carbon tetrachloride", Optical Materials Express 9 (5), 2264 (2019), doi:10.1364/OME.9.002264.

[13] W. P. Putnam et al., "Few-cycle, carrier-envelope-phase-stable laser pulses from a compact supercontinuum source", J. Opt. Soc. Am. B 36 (2), A93 (2019), doi:10.1364/JOSAB.36.000A93.

[14] M. Vengris, N. Garejev, G. Tamošauskas, A. Čepėnas, L. Rimkus, A. Varanavičius, V. Jukna & A. Dubietis, "Supercontinuum generation by co-filamentation of two-color femtosecond laser pulses", Scientific Reports Volume 9, Article number: 9011 (2019).

[15] M. Yu et al., "Coherent two-octave-spanning supercontinuum generation in lithium-niobate waveguides", Opt. Lett. 44 (5), 1222 (2019), doi:10.1364/OL.44.001222.

[16] Mariusz Klimczak, Damian Michalik, Grzegorz Stępniewski, Tanvi Karpate, Jarosław Cimek, Xavier Forestier, Rafał kasztelanic, Dariusz Pysz, Ryszard Stępień, and Ryszard Buczyński, "Coherent supercontinuum generation in tellurite glass regular lattice photonic crystal fibers", J. Opt. Soc. Am. B 36(2) A112-A124 (2019).

[17] Mariusz Klimczak, Bartłomiej Siwicki, Alexander Heidt, and Ryszard Buczyński, "Coherent supercontinuum generation in soft glass photonic crystal fibers", Photon. Res. 5(6) 710-727 (2017).

[18] Anna G. Ciriolo, Matteo Negro, Michele Devetta, Eugenio Cinquanta, Davide Faccialà, Aditya Pusala, Sandro De Silvestri, Salvatore Stagira, and Caterina Vozzi, "Optical Parametric Amplification Techniques for the Generation of High-Energy Few-Optical-Cycles IR Pulses for Strong Field Applications", MDPI APPLIED SCIENCES, MARCH8 2017.

[19] E. A. Migal, F. V. Potemkin, and V. M. Gordienko, "Highly efficient optical parametric amplifier tunable from near-to mid-IR for driving extreme nonlinear optics in solids", Optics Letters, Vol. 42, Issue 24, pp. 5218-5221, 2017.

[20] Chaohua Wu, Jingtao Fan, Gang Chen, and Suotang Jia, "Symmetry-breaking-induced dynamics in a nonlinear microresonator", Opt. Express 27(20), 28133-28142 (2019).

[21] Sung Bo Lee, Hyeon Sang Bark, and Tae-In Jeon, "Enhancement of THz resonance using a multilayer slab waveguide for a guided-mode resonance filter", Opt. Express 27(20), 29357-29366 (2019).

[22] Houssein El Dirani, Laurene Youssef, Camille Petit-Etienne, Sebastien Kerdiles, Philippe Grosse, Christelle Monat, Erwine Pargon, and Corrado Sciancalepore, "Ultralow-loss tightly confining Si3N4 waveguides and high-Q microresonators", Opt. Express, Vol. 27, Issue 21, pp. 30726-30740 (2019).

[23] Ivan S. Maksymov; Andrey A. Sukhorukov; Andrei V. Lavrinenko ; Yuri S. Kivshar, "Comparative Study of FDTD-Adopted Numerical Algorithms for Kerr Nonlinearities", IEEE Antennas and Wireless Propagation Letters, Year: 2011 | Volume: 10 | Journal Article | Publisher: IEEE.

[24] Kaikai Xu, Silicon MOS Optoelectronic Micro - Nano Structure Based on Reverse - Biased PN Junction, Physica Status Solidi-A Applications and Materials Science (PSS-A), Volume 216, Issue 7, April 10, 2019.

[25] Ozum Emre Asirim, Mustafa Kuzuoglu, "Optimization of optical parametric amplification efficiency in a microresonator under ultrashort pump wave excitation", International Journal of Electromagnetics and Applications, November 2019.

[26] Ozlem Ozgun, Mustafa Kuzuoglu, Metamaterials and Numerical Models, Nova Novinka; UK ed. Edition, 2011.

[27] Ozlem Ozgun, Mustafa Kuzuoglu, MATLAB-based Finite Element Programming in Electromagnetic Modeling, CRC Press, 1st edition, 2018.